A novel mitochondrion-related organelle and complex endosymbiosis in a rare anaerobic single-celled predator

Ivan Čepička

ivan.cepicka@natur.cuni.cz

Charles University, Czechia https://orcid.org/0000-0002-4322-0754

Ondřej Pomahač

Charles University, Czechia https://orcid.org/0000-0003-0508-6803

Daniel Méndez-Sánchez

University of Warszaw

Yong Heng Phua

Okinawa institute of science and technology

Linus Zeller

Max Planck Institute for Marine Microbiology

Marek Valt

Charles University

Kateřina Koštířová

Charles University

Bruno Humbel

Okinawa institute of science and technology

Filip Husnik

Okinawa institute of science and technology

Article

Keywords:

Posted Date: April 29th, 2026

DOI: https://doi.org/10.21203/rs.3.rs-8743768/v1

Additional Declarations: There is **NO** Competing Interest.

A novel mitochondrion-related organelle and complex endosymbiosis in a rare anaerobic single-celled predator

Ondřej Pomahač[1,*,#], Daniel Méndez-Sánchez[1,2,3,#], Yong Heng Phua[3,#], Linus Matz Zeller[4], Marek Valt[1], Kateřina Koštířová[1], Bruno M. Humbel[3], Filip Husník[3], Ivan Čepička[1,*]

1 Department of Zoology, Faculty of Science, Charles University, Viničná 7, 128 00 Prague, Czech Republic

2 Institute of Evolutionary Biology, Faculty of Biology & Biological and Chemical Research Centre, University of Warsaw, Warszawa 02-089, Poland

3 Okinawa Institute of Science and Technology, Okinawa, 904-0495, Japan

4 Max Planck Institute for Marine Microbiology, Celsius Strasse 1, D-28359, Bremen, Germany

co-first authorship

Email: ondrej.pomahac@natur.cuni.cz, ivan.cepicka@natur.cuni.cz

Abstract

Anaerobic single-celled eukaryotes illustrate the remarkable diversity of adaptations to life without oxygen, including multiple mitochondrial reductions and various symbiotic interactions with prokaryotes. However, rare lineages remain virtually unexplored. From 11 collected cells, we conducted an in-depth investigation of the ciliate *Legendrea loyezae*, a rare predator of microscopic animals. Using single-cell transcriptomics and metagenomics, we generated a high-completeness host transcriptome and macronuclear genome and characterized a novel type of mitochondrion-related organelle. By integrating omics data with microscopy and 3D imaging, we uncover an exceptionally complex endosymbiotic consortium with two methanogenic archaea and two bacteria, including the first strictly anaerobic member of *Legionellales*, and the most reduced member of *Thermodesulfobacteriota*, with a 0.5-Mb genome. We infer the metabolic potential and extensive complementarity within this pentapartite system and align it with spatial relationships. Our results expand the known complexity of anaerobic eukaryotes and demonstrate the feasibility of comprehensive analyses of rare protists.

Introduction

Oxygen-depleted environments pose a daunting evolutionary challenge for eukaryotes, necessitating a reorganization of fundamental metabolic processes. Mitochondrial streamlining and intimate prokaryotic symbioses have therefore become central themes in the biology of anaerobic microbial eukaryotes[1–3]. Single-celled eukaryotes, and especially ciliates, have become widely used as model organisms, since multiple lineages have independently undergone anaerobiosis, metabolic by-passing, and acquisition of prokaryotic symbionts[4–11]. Methanogenic Archaea represent the most studied symbionts of anaerobic protists due to their environmental impact[12,13]. Recently, multipartite symbioses in ciliates (Alveolata), parabasalids (Metamonada), and other protists have been gaining attention due to their metabolic complexity[10,13–17] greatly

surpassing the metabolic complexity of intracellular symbioses in animals. So far, the most complex endosymbiotic consortium described in detail is the multipartite system in *Pelomyxa* amoeba, where a methanogenic archaeon and two syntrophic bacteria play crucial metabolic roles[17]. Due to vertical transmission, endosymbionts typically undergo substantial genome reduction, functional specialization, and cellular integration. Long-term heritable endosymbionts then follow the path of prokaryotic-derived organelles, becoming highly specific and dependent on their hosts[1,2,18–20].

The model anaerobic ciliates have been selected primarily from easily culturable, bacterivorous species that can be maintained in dense cultures, such as members of the classes Armophorea and Plagiopylea[4,8,21]. Recent studies have revealed the variety of endosymbiotic methanogenic or ectosymbiotic sulfate-reducing prokaryotic partners of these ciliates[8,11]. The common basis of these widespread symbioses is hydrogen scavenging and parallel reductions of mitochondria into so-called hydrogenosomes or hydrogen-producing mitochondria[6,7,22,23]. Consequently, hydrogenase, the enzyme that catalyzes the formation of molecular hydrogen, is considered a general feature of reduced mitochondria of anaerobic ciliates, and its absence from the data is attributed to insufficient depth of sequencing and limitations of single-cell methods[6–8,24,25].

Here, we studied a rare and unculturable ciliate, *Legendrea loyezae* (class Litostomatea). This bizarre, predatory, anaerobic, tentaculiferous ciliate can be viewed as an apex predator in its hypoxic niche, as its prey are microscopic metazoans, specifically gastrotrichs[26]. Single-cell amplicon sequencing of *Legendrea* species*,* using the 16S rRNA gene universal prokaryotic primer set, has previously revealed the presence of its potential symbionts belonging to methanogenic Archaea and Syntrophaceae bacteria[26]. Using single-cell metagenomics and transcriptomics, along with advanced single-cell microscopy on only 11 *Legendrea* cells, we have uncovered an unusual and currently the most complex symbiotic consortium in an anaerobic eukaryote, comprising four prokaryotic symbionts: two archaeal methanogens (a hydrogenotrophic and an acetoclastic one, respectively) and two bacterial partners (a propionate oxidizer and a carbohydrate fermenter). We describe the prokaryotic consortium of *Legendrea loyezae* at the spatial, genomic, and metabolic levels and propose a novel type of ATP-producing anaerobic mitochondrion lacking a hydrogenase. We demonstrate that integrating single-cell methods for unculturable and rare eukaryotes allows the reconstruction of even highly complex symbiotic consortia.

Results

Structure of the symbiotic consortium of *Legendrea loyezae*

Using single-cell methods, we found that the ciliate (cell volume approx. 50,000 μm^3, n=1) harbors four different prokaryotes, which form a complex pentapartite symbiosis with the host (Fig. 1). The consortium is formed by two Archaea, *Candidatus* Methanothrix pelomyxae (Methanosarcinales, 346 cells, n=1) and *Methanobacterium* sp. (Methanobacteriota, 2970 cells, n=1), and two bacteria, for which we propose provisional names *Candidatus* Xociella bifrons (Gammaproteobacteria, 874 cells, n=1) and *Candidatus* Syntrophilus obsequens (Syntrophia, 605 cells, n=1). All four prokaryotes are located directly in the host cytoplasm, without a membrane of host origin (Figs. 1-3 and S1). To reconstruct the topological relationships, we employed transmission electron microscopy (TEM), fluorescence *in situ* hybridization (FISH), 3D reconstruction using focused ion beam-scanning electron microscopy (FIB-SEM), as well as nearest-neighbor statistical methods based on random labeling and a complete spatial randomness (CSR) framework. CSR analysis clearly shows that the symbiotic consortium is not randomly dispersed in the host (Table S1). It is clearly structured around *Methanobacterium* sp. as the main hub, with the significantly shortest distance from other prokaryotic partners (Table S1). *Ca*. S. obsequens and *Methanobacterium* sp. form parallelly aligned clusters detectable across different methods: fluorescence microscopy (a combination of autofluorescence and FISH, Figs. 1a, f, g and S1b), TEM, and FIB-SEM (Figs. 1h, 2d, S1, and Movie S1). Statistical analysis confirms the strongest affinity between these two species among the symbionts (Table S1). Most of the cells of *Ca*. M. pelomyxae are localized around or within the clusters of the above-mentioned symbionts (Figs. 1b, e, h, S1a, e). However, all methods also show an accumulation of *Ca*. M. pelomyxae cells in the oral basket (buccal area) of the host, together with a fraction of cells of *Methanobacterium* sp. (Figs. 1b, e, 2c and S1a, e). Only a minor portion of *Ca*. X. bifrons cells seem to participate in the clusters of the above-mentioned symbionts, with most cells occupying the periphery of the host cell, with the highest abundance posteriorly (Figs. 1c, e, h, 2a-c). The majority of the host's mitochondrion-related organelles (MROs) are also dispersed on the cell periphery, posteriorly, but also in tentacles, unlike the prokaryotes (Figs. 1i, j, 2b and S1d). Atypically for anaerobic ciliates, the MROs are not directly associated with any of the symbionts (Figs. 1h, 2a-c and S1d).

Genomics of the symbiotic consortium

After binning the metagenomic assembly of *Legendrea loyezae*, we identified five prokaryotic metagenome-assembled genomes (MAGs) and one complete circular prokaryotic genome. We decided to work with three complete or nearly complete MAGs that have the highest coverage. The two other MAGs having the lowest completeness and coverage related to *Trichorickettsia* and *Tisiphia* (both Pseudomonada), both known animal parasites, were considered contaminants likely associated with the prey, as several ribosomal rDNA sequences belonging to gastrotrichs were obtained (Table S2). We also recovered several gastrotrich ribosomal rDNA sequences from the transcriptomic data of *L. loyezae* (Table S2). On the other hand, we did not find any ciliate sequences except those of *L. loyezae* in both datasets, which strongly suggests that gastrotrichs are the primary prey of this predatory ciliate.

Candidatus Syntrophilus obsequens

Based on 16S rRNA gene phylogeny, *Ca*. S. obsequens is divergent from other members of Syntrophaceae, with less than 90% nucleotide identity to the closest relatives (Fig. 3a). We obtained the 0.53 Mbp circularized single-contig genome with a completeness of 98% (contamination 0.2%) and a GC content of 24% (Fig. 3a, c). This genome is the most reduced Syntrophaceae genome known to date, as well as the most reduced symbiont of the consortium (Fig. 3c, d). The genome is almost ten times smaller than that of the related endosymbiont, *Ca.* Syntrophus pelomyxae from the amoeba *Pelomyxa schiedti* (Amoebozoa: Archamoebae), which is 4.97 Mbp[17]. The significant reduction is apparent throughout the entire genome in terms of clusters of orthologous groups (COGs) (Fig. 3b). The least reduced is the COG category containing transcription-related genes. Interestingly, DNA polymerase III appears to be composed solely of an alpha subunit, representing an extreme reduction comparable only to the most reduced symbionts known[27]. *In silico* reconstruction of the reduced metabolic pathways revealed that the backbone of its energetic metabolism is the anaerobic propionate/butyrate oxidation pathway (Fig. 4), with the ability to use, most likely, propionate and, likely, also long-chain fatty acids as substrates. Propionate usage is supported by the presence of the CoA transferase enzyme (CoA transferase), which, based on our phylogenetic analysis, is closely related to that of *Smithella* spp. (Fig. S2). In *Smithella propionica*, the ability to utilize propionate was experimentally confirmed[28]. The genome of *Ca*. S. obsequens encodes two thiolases, suggesting that it undergoes Claisen condensation of propionyl-CoA into acetyl-CoA and butyryl-CoA, which are subsequently oxidized to acetate. This pathway is well-documented in *Smithella propionica*[28]. The only other activation enzyme is a long-chain fatty acid ligase, likely enabling the utilization of fatty acids from the host's gastrotrich prey. Interestingly, the bacterium lacks a typical kinase for substrate-level phosphorylation and ATP production. However, the terminal conversion of acetyl-CoA to acetate is performed by reversible ADP-forming acetyl-CoA synthase, which completes the beta-oxidation pathway using a minimized protein toolkit. Redox balance can be maintained primarily through hydrogen release via cytosolic FeFe-hydrogenase (Hnd), alternatively through periplasmic NiFe-hydrogenase, or via a bidirectional redox shuttle – succinate dehydrogenase/fumarate reductase. Nitric oxide, if available, can likely be reduced to nitrous oxide as an electron acceptor alternative to hydrogen ions or fumarate. The primary metabolic products are acetate and hydrogen.

Candidatus Methanothrix pelomyxae

The methanogen was identified as Ca. *M. pelomyxae* based on its identical 16S rRNA gene sequence to KX156800[29], which was described as a symbiont of the giant anaerobic amoeba, *Pelomyxa palustris* (Amoebozoa: Archamoebae) (Fig. 3e). The MAG comprises 123 contigs with a total length of 2.5 Mbp, a completeness of 99.4% (contamination 0.2%), and a GC content of 50% (Fig. 3g). In contrast to the acquired draft genomes of the two bacterial symbiotic partners of *L. loyezae*, the genome of *Ca.* M. pelomyxae is not significantly reduced in size (~10%) and number of CDS (~13%) compared to its free-living relatives (Fig. 3f, h). The *in silico* reconstruction of the energetic metabolism showed that, like other *Methanothrix* (syn. *Methanosaeta*) species[30], the symbiont is with high certainty a strictly acetoclastic methanogen, utilizing acetate as its sole energy and carbon source (Fig. 4). Interestingly, the MAG encodes four paralogs of a CoA transferase, related to the enzyme from *Ca.* Syntrophilus obsequens (Fig.

S2). The presence of a sulfide detoxification mechanism involving sulfide dehydrogenase, sulfurtransferase, and thioredoxin is likely important to the consortium (Fig. 4). It is proposed to be unique among methanogenic Archaea[31] and thus could be beneficial to *Methanobacterium* sp. in the vicinity. In this species, we detected no autofluorescence signal under UV light, a typical feature for most methanogens with a high F420-coenzyme pool, which is consistent with the findings from *Pelomyxa palustris*[29].

***Candidatus* Xociella bifrons**

Based on the 16S rRNA gene phylogeny, the bacterium clusters within a highly supported group of uncultured *Coxiellaceae*, which is sister to the rest of *Coxiellaceae* diversity, although with low statistical support (Fig. 3i). The MAG consists of 167 contigs with a total length of 1.2 Mbp, a completeness of 96.5% (contamination 0.8%), and a GC content of 38%. The genome of *Ca*. X. bifrons is approximately 40% smaller compared to that of published members of *Coxiellaceae* (around 2 Mbp) (Fig. 3k). The bacterium is likely an energy parasite, scavenging ATP via ATP/ADP translocase (Tlc1). In addition, carbohydrates likely represent its main alternative energy source. The complete glycolytic pathway is encoded in the genome. The bacterium also encodes an operon for leucine degradation. ATP is generated by two acetate/propionate kinases. The bacterium lacks an electron transport chain and thus relies on fermentation with acetate and likely propionate as the main products. These features make the bacterium the first reported strictly anaerobic member of the otherwise aerobic order, *Legionellales*[32]. FeFe hydrogenase serves as a redox balancing mechanism by producing hydrogen. Interestingly, the MAG encodes a four-subunit sulfhydrogenase complex (two subunits of NiFe hydrogenase and two subunits of sulfide reductase). The complex is likely capable of transferring electrons from NAD(P)H as well as hydrogen and producing sulfide, similarly to the complex of *Pyrococcus*[33]. It broadens the bacterium's redox balancing capabilities and makes it less dependent on hydrogen scavengers. The bacterium appears to possess a type IV secretion system typical of *Coxiella* or *Legionella* (Fig. 4). However, unlike *Coxiella*, it does not occur in vesicles in the host's cytoplasm (Fig. 1h).

***Methanobacterium* sp.**

Only a partial 16S rRNA gene sequence was retrieved from the metagenome, but a complete sequence was extracted from the transcriptomic data and is identical to that of the undescribed methanogens from *Legendrea pespelicani*[26] and a metopid ciliate, *Castula fusca*[11], respectively. Phylogenetically, *Methanobacterium* sp. is closely related to methanogens from several undescribed symbionts of metopid ciliates[11] (Fig. S3). In contrast to the other three symbionts, we obtained only 251 low-coverage genome fragments, totaling approximately 0.7 Mbp in length, with a completeness of 24.3% and a GC content of 33.9%. Although we obtained only a fragment of the genome, its central energy metabolism is certainly the standard hydrogenotrophic methanogenesis. We identified several genes involved in hydrogen uptake and methanogenesis in the genomic fragment, as well as in the transcriptomic data (Table S3). Moreover, the strong autofluorescence, a reliable indicator of a high pool of oxidized F420-coenzyme[34], clearly indicates active hydrogenotrophic methanogenesis in *Methanobacterium* sp. (Figs. 1f, g and S1b).

New type of mitochondrion-related organelles (MRO)

In the *Legendrea* cell, we have identified the putative MROs as small irregularly-shaped oblong vesicles (length, avg = 1.06 μm, std = 0.14, range = 0.78 - 1.46 μm; diameter, avg = 0.32 μm, std = 0.05, range = 0.45 - 0.24 μm, n = 30) concentrated mainly on the periphery of the cytoplasm (Figs. 1i, j, 2b and S1d). Morphologically, they are different from classic spheroidal to ellipsoidal hydrogenosomes known from Armophorea (e.g., *Nyctotherus*) and other anaerobic ciliate classes[6,7,12,22]. The outer membrane is likely present; however, the cristae appear to be absent (Fig. 1j).

We have predicted the proteome and metabolic pathways of this ATP-producing MRO without hydrogenase (Fig. 5) based on the single-cell transcriptomes (data from 3 cells combined, 17,239 filtered transcripts, BUSCO 48.0%) and metagenomes (data from 2 cells combined, 2,621 filtered contigs, total size 32.6 Mbp, BUSCO 83.6%) of *L. loyezae* and corroborated the results with the transcriptomes of a closely related, undescribed free-living anaerobic litostomatean, a spathidiid referred to as SIVAB (data from 3 cells combined, 18,477 transcripts (filtered >500 bp), BUSCO 81.3%; Fig. S4). In the metagenome of *Legendrea loyezae,* we could not detect any trace of the mitochondrial genome or any remnants of the electron transport chain, except for soluble fumarate reductase (normally part of Complex II), which is encoded in the nuclear genome. In total, we identified 60 proteins in *L. loyezae* and SIVAB ciliate that are predicted to be transported to the MRO, and corroborated the targeting signal (Table S4). Unexpectedly, we did not find the canonical ciliate hydrogenase with the typical structure (HydA-NuoE-NuoF fused gene) or any fragment or other relevant candidate for an MRO hydrogenase in any of the datasets, despite their high completeness. In contrast, we identified hydrogenases of all prokaryotic partners except for the highly fragmented *Methanobacterium* sp. assembly. The only identified redox route for the regeneration of NAD+ from NADH is the reversed truncated TCA cycle, involving clearly targeted malate dehydrogenase, and likely fumarate hydrolase and fumarate reductase, with a dubious targeting signal (Table S4). The other branch of the former TCA cycle, including 2-oxoglutarate dehydrogenase (OGDH) and succinate-CoA synthase (SCS), supplies succinyl-CoA for ATP generation.

We identified the typical MRO enzyme of energetic metabolism, acetate CoA transferase (ASCT), in both *L. loyezae* and SIVAB ciliate. Subsequent phylogenetic analysis of ASCT placed all detectable paralogs within the clade with other ciliates in the dataset, strongly suggesting it is a typical acetyl-CoA: succinate CoA transferase known from other anaerobic ciliates (Fig. S2). The MRO thus likely performs the canonical ASCT–SCS cycle described earlier[35], converting acetyl-CoA, derived from the NADH-dependent pyruvate dehydrogenase complex, to acetate.

The MRO likely maintains a well-supported, yet noncanonical pathway for degradation of branched-chain amino acids (BCAAs), specifically valine and isoleucine (Fig. 5). The valine pathway terminates at the propionyl-CoA step, lacking the enzymes propionyl-CoA decarboxylase (PCD) and methylmalonyl-CoA mutase (MMM). Consequently, the pathway is not connected to succinyl-CoA production. The two enzymes appear to be absent from model ciliates, such as *Tetrahymena*[36], but are predicted to be present in *Nyctotherus*[35]. We conclude that propionyl-CoA is utilized as a substrate for energy production by ASCT, and thus, the final products of MRO metabolism are propionate, acetate, malate, and succinate (Fig. 5).

The complete cytosolic glycolytic pathway is present, starting with glucokinase (GK). Interestingly, as the first report in a ciliate, pyrophosphate-dependent phosphofructokinase is present, in addition to the usual ATP-dependent phosphofructokinase. Surprisingly, the MRO also

encloses two reactions of the glycolytic pathway involving phosphoglycerate mutase (PGM) and enolase (ENO), and later deviates from the standard pathway with phosphoenolpyruvate carboxylase kinase (PEPCK) and malate dehydrogenase (MDH) (Fig. 5). From targeting prediction, it is unclear whether fumarase and fumarate reductase/succinate dehydrogenase are effective in the MRO, as they lack a clear signal (Table S4). However, both enzymes are present in the studied transcriptomes and metagenome, and we consider them to be more likely mitochondrial, consistent with other known MROs[6,7,23,35]. In that case, the glycolytic steps are connected with the reversed truncated TCA cycle, and the released end product is then succinate. The OGDH then feeds into SCS. Excess malate is transported to the cytoplasm and converted by malic enzyme (two paralogs have been detected) into pyruvate, which is then imported back into the MRO. This split enables 3-phosphoglycerate (3-PG) to serve as a partial substrate in standard glycolytic steps in the cytoplasm and partially to alleviate the redox burden in the MRO. In the MRO, phosphoenolpyruvate (PEP) is converted to oxaloacetate with PEPCK, gaining one molecule of GTP, and one molecule of NADH is oxidized in the subsequent step. The reaction of PEPCK in the carboxylation direction also assimilates one molecule of carbon dioxide, a process that has been experimentally proven to be favorable under reductive conditions[37]. Subsequent malate export eases the MRO for one reduced equivalent, with a stoichiometry of one malate molecule per one NADH molecule. If fumarase and fumarate reductase are active in the MRO, and succinate is subsequently exported, it results in the oxidation of another molecule of NADH (Fig. 5).

The most important transporters for di- and tricarboxylic acids were identified under the generic designation SLC25 or 2-oxoglutarate/malate antiporters. Transporters for sugar compounds have not been well characterized yet; however, the MRO predicted proteome contains multiple annotated mitochondrial transporters. ATP is exported via ATP/ADP carriers. We did not find any trace of the mitochondrial outer membrane complex proteins. On the contrary, we identified several proteins of the inner membrane complex and protein processing, including TIM17, TIM50, Hsp60, and processing peptidase alpha and beta subunits (Fig. 5).

Protologues

Candidatus Syntrophilus gen. nov.
[Syn.tro'phi.lus], from Gr. prefix *syn-* = together; Gr. *trophē* = nourishment; N.L. masc. n. *Syntrophilus* – companion in syntrophy.

The description is the same as for the type species, *Ca*. Sytnrophilus obsequens.

Candidatus Syntrophilus obsequens sp. nov.
obsequens [ob'se.quens]. L. adj. *obsequens* – compliant, obliging, yielding.
Strictly anaerobic propionate/butyrate-oxidizing bacterium; rod-shaped; intracellular; defined by 16S rRNA gene sequence (accession number XXXXXX in NCBI).

Candidatus Xociella gen. nov.
[So.si.el'la], from Nahuatl root *xoc-* = sour, acidic; connecting vowel *-i-*, N.L. fem. dim. suffix *-ella*; N.L. fem. n. *Xociella* – the small acidic one).

The description is the same as for the type species, *Candidatus* Xociella bifrons.

Candidatus Xociella bifrons sp. nov.
bifrons [bi'frons]; L. *bifrons* – two-faced, deceitful.
Strictly anaerobic fermenting and ATP-scavenging bacterium; rod-shaped; prominent black core in TEM preparations; intracellular; defined by 16S rRNA gene sequence (accession number XXXXXX in NCBI).

Candidatus Methanothrix pelomyxae (syn. *Candidatus* Methanosaeta pelomyxae)
Strictly anaerobic acetoclastic methanogenic archaeon; rod-shaped, rectangular in a longitudinal section; prominent longitudinal septum; intracellular; defined by 16S rRNA gene sequence (accession number KX156800 in NCBI)[29].

Discussion

As *Legendrea loyezae* is a rare organism, we have studied only 11 cells from two populations of this peculiar ciliate over the course of several years (Table S5). Nevertheless, we were able to reconstruct the most complex endosymbiotic consortium known to date solely using single-cell methods. We provide an in-depth overview of the spatial and metabolic interactions among the symbionts and predict the host ciliate's MRO metabolism (Fig. 5). Our work clearly demonstrates that integrating single-cell imaging and omics methods allows for metabolic reconstructions and detailed studies of rare and non-model microorganisms, yielding valuable discoveries (Fig. 4). On the other hand, we also acknowledge the limitations of these methods, particularly the need for a deeper understanding of the metabolic and ultrastructural aspects of MROs in spathidiids and anaerobic Litostomatea, which necessitates the use of more robust experimental methods.
By most definitions, *Legendrea loyezae* is practically the opposite of a model organism. Anaerobic spathidiid ciliates are predators of other unicellular or microscopic, multicellular eukaryotes. Hence, from an ecological perspective, the predicted MRO without oxygen-sensitive hydrogenase may allow them the leeway to hunt other eukaryotic prey close to the oxycline and uniquely exploit microaerotolerant, yet likely aerobic prey (i.e., gastrotrichs in the case of *L. loyezae*). Moreover, the ciliate cells host a completely anaerobic, multipartite symbiotic consortium, which is uniquely rich not only in the species involved and their numbers, but also in predicted metabolic interactions among them, compared to the anaerobic ciliates or other eukaryotes that have been studied so far. The presence of symbiotic prokaryotes is likely stable in the ciliate, as evidenced by the genome reduction of *Ca.* Syntrophilus obsequens and *Ca.* Xociella bifrons, suggesting their dependence on the host. We further corroborated the presence of the symbionts in several *L. loyezae* cells by different methods (single-cell metagenome, single-cell transcriptome, and single-cell FISH of two populations). *Ca.* Methanothrix pelomyxae is the only previously reported symbiotic member of the genus[29].

In the molecular data of *L. loyezae* and SIVAB spathidiid, we did not find any trace of the mitochondrial outer membrane complex proteins. Our results imply an unusual organization of its outer membrane transport system. We successfully characterized the main energetic and redox metabolism of the MRO, which is essential, as most known symbioses of prokaryotes and

anaerobic ciliates are associated with hosts' MROs[6,7,12]. At least a partial electron transport chain has been retained in most of the anaerobic ciliate taxa from various groups[6,7,23,35]. However, this is not the case in *L. loyezae* and SIVAB spathidiid, which is consistent with members of the unrelated class Plagiopylea, where the mitochondrial genome has also been lost[6]. Having extracted the partial mitochondrial genome of the gastrotrich prey from the metagenomic data of *L. loyezae* and identified several transcripts of the gastrotrich's electron transport chain in the transcriptomic data, we consider it highly unlikely that any remnants of a possible mitochondrial genome of *L. loyeza*e were undetected.

In all thoroughly studied groups of anaerobic ciliates across different classes, a typical tripartite hydrogenase is present in the MROs[6,7,23,35]. This presence has been considered universal among anaerobic ciliates to date. Yet, it has not yet been clearly proven in rumen ciliates (Trichostomatia), the close endobiotic relatives of *Legendrea*. The absence of hydrogenase in *L. loyezae* (and SIVAB) contrasts with the idea of its universal presence in anaerobic ciliates. The ciliate relies entirely on the alternative NAD+/NADH management related to malate and succinate metabolism, which has been described in other anaerobic ciliates, e.g., *Nyctotherus ovalis* [22,35], and in several variants in other protists or even metazoans[38]. Thus far, it has been considered auxiliary in anaerobic ciliates, and the research focus has primarily been on the hydrogenase and hydrogen management[6,7,23,35]. A functionally parallel system, utilizing succinate as the redox product, is also known in some other protists, for example, the procyclic stage of *Trypanosoma brucei* (Discoba: Euglenozoa)[39]. Whether this redox-balancing system is self-sustainable in ciliates and how many syntrophic partners are involved in it needs to be investigated and proven experimentally. The transfer of 3-phosphoglycerate into the MRO is unusual but resembles the glycosome transport in trypanosomatids[40]. Although glycosomes, peroxisome-derived compartments for glycolysis, have been extensively studied in *Trypanosoma*, the carrier for 3-PG has yet to be described.

Currently, *Legendrea* is not a suitable model organism for these studies due to its relative rarity. However, the resemblance to known anaerobic MROs and glycosome-like product transport gives strong biological plausibility to our prediction. The localization of MRO on the periphery of the host cell cytoplasm is consistent with the production of acidic compounds, such as succinate, as they are more easily released into the environment. This prevents the acidification of the cytoplasm, which could block critical metabolic enzymes in the cell, e.g., dehydrogenases[41]. The absence of any hydrogen scavengers around these putative MROs itself strongly contradicts any known hydrogenosome organization in a freshwater ciliate, as the cytoplasmic endosymbiotic hydrogenotrophic methanogens (e.g., *Methanobacterium*) are in all well-documented cases in a tight association with a hydrogenosome[6,11,12]. Given the current results, the predicted MRO represents a novel type of reduced mitochondrion-related organelle, lacking hydrogenase, which releases malate, succinate, acetate, and propionate as fermentation and redox products, thereby expanding the scope of research on MROs in anaerobic ciliates and eukaryotes in general. We cannot fully reject the possibility of the presence of a hydrogenase, but in that case, it would have to be unusually divergent for it to have remained undetected by the annotation and sequence-alignment methods we used. However, the presence of such a divergent hydrogenase itself would be as significant a finding as the absence.

For the spatial statistics, we decided to use a tailored method of directed nearest-neighbour (NN) distances per symbiont cell surface. We believe that this approach better preserves the biological signal most relevant to diffusion-limited metabolite exchange. It revealed that the spatial relationships among the symbionts are consistent with their predicted functions in the system and their metabolic capacities. Importantly, the hydrogenotrophic methanogen, *Methanobacterium* sp., is not visibly associated with MROs, which further corroborates that the latter does not produce hydrogen, but is preferably associated with *Ca*. S. obsequens and partially with the other two prokaryotes. The observed spatial organization of the symbiotic consortium of *L. loyezae* resembles that of free-living syntrophic consortia in granular sludge, where acetate-producing propionate/butyrate oxidizers and hydrogenotrophic methanogenic Archaea cluster together, acetoclastic methanogens are associated in their proximity, and carbohydrate fermenters producing propionate/butyrate and acetate form an outer layer[42]. Moreover, it was also demonstrated that this structure corresponds to the scenario when carbohydrates are fed to the fermenters[42]. When volatile fatty acids are added, the layer structure reconfigures into decentralized clusters, preserving the lower-level spatial relationships. Considering that *L. loyezae* feeds on small metazoans[26], the global structure of the consortium can likely change during the different stages of digestion. It suggests that the metabolic interactions shape the spatial structure of the consortium, even at the level of a single host cell (Fig. 4).

Ca. S. obsequens requires intimate proximity with a hydrogenotrophic methanogen, *Methanobacterium* sp., as fatty acid oxidation is endergonic without preserving the partial pressure of produced hydrogen at low levels[43]. Another possible hydrogen source can be the *Ca.* X. bifrons while performing fermentation, or *Ca.* M. pelomyxae, as there is experimentally proven "leakage" of hydrogen from a *Methanothrix* species[44]. The observed proximity of *Ca.* M. pelomyxae and *Methanobacterium* sp. (Fig. 2) can be partially explained by the exchange of carbon dioxide produced by *Ca.* M. pelomyxae, which is the main carbon source for *Methanobacterium* sp. (Fig. 4), or by their cooperation in the detoxification of sulfide. The main function of *Ca.* M. pelomyxae in the consortium is the sink for the produced acetate (Fig. 4), as *Methanothrix* has a high affinity to acetate and tolerates high acetate concentrations at the same time[45,46]. *Ca.* M. pelomyxae is thus a very effective acetate sink also for the carbohydrate-fermenting *Ca.* X. bifrons and the host's MROs, which are located on the periphery of the host cell. Besides acetate, *Ca.* X. bifrons is likely capable of propionate production from leucine degradation. MROs also generate acetate and, more importantly, propionate, which is the main substrate for *Ca.* S. obsequens (Fig. 4). Due to the absence of hydrogenase in the MRO, a partnership with a hydrogenotroph is not required. However, the constant removal of acetate and propionate as fermentation products is desirable. Thus, from the host's perspective, the consortium primarily functions as a propionate sink (*Ca.* S. obsequens) and an acetate sink (*Ca.* M. pelomyxae), offering the host the most significant benefits (Fig. 4).
The nature of the symbiosis of *Ca.* X. bifrons and the host is rather a form of energetic parasitism, while the potential benefits for the host from the interaction remain unclear. As the bacterium is generally localized relatively near MROs at the periphery of the host's cytoplasm, the ATP-scavenging remains the most likely strategy. Interestingly, the bacterium and MRO appear to be complementary in the degradation of branched-chain amino acids, valine and isoleucine in the MRO, and leucine in *Ca.* X. bifrons, respectively. This suggests at least a possibility for

metabolic flexibility, and also, limited mutualistic metabolite exchange cannot be excluded. We note that our analysis, although using combined methods, is based on only a few cells studied in detail (Figs. 1, 2 and Table S5) and several other cells examined using fluorescence methods. Still, we consider our interpretation to be the most parsimonious explanation of the given data within the context of the entire symbiotic consortium and contextual metabolic pathways and products of the individual organisms.

CoA transferases are important enzymes that connect the entire community. At the same time, they are among the most difficult to interpret correctly. First, various authors have shown their substrate promiscuity[47–49]. Second, we lack experimental confirmations for many types of enzymes in eukaryotes, and the annotations in databases are often ambiguous. Based on our annotations and phylogenetic relationships of several types of CoA transferases (Fig. S2), we conclude that all four CoA transferases of *Ca.* M. pelomyxae are related to enzymes characterized in *Fasciola hepatica* and predicted as acetate CoA transferases with promiscuous CoA donors in succinate or propionate[50] or with propionate as a possible acceptor[49]. Their likely function is to activate acetate to acetyl-CoA without ATP consumption, which would be advantageous when compared to the AMP-forming acetyl-CoA synthase. Another possible use is as an auxiliary supply of propionate for *Ca.* S. obsequens, since it uses a transferase from the same family, acetyl-CoA hydrolase/transferase family enzyme (ACH1), in which propionate or butyrate serves as the acceptor of CoA, while acetyl-CoA or possibly succinyl-CoA acts as the donor. We hypothesize that it is the only way to activate short fatty acids encoded in its reduced genome. The activation of propionate has been experimentally confirmed for the related acetate-producing species, *Smithella propionica*, co-cultured with a methanogen, *Methanospirillum hungatei*[51]. CoA transferases of *L. loyezae* and SIVAB ciliate cluster with those of other ciliates (Fig. S2). Nevertheless, the characterization of the enzyme in ciliates remains unclear. Based on experiments carried out in the anaerobic ciliate *Nyctotherus ovalis* (Armophorea), the CoA transferase behaves as succinate CoA transferase with acetate as CoA donor, so-called ASCT; however, it is not closely related to the ASCT 1B or 1C known from other anaerobic protists (Fig. S2)[52]. Automated annotators classify it mostly as 3-ketoacid CoA transferase, which is likely inaccurate, or the enzyme is promiscuous on the donor and acceptor side. We follow the experimental results on ASCT of *T. brucei*, which is closely related to the ciliate ASCT in our analysis, and interpret the enzyme in a broad functional sense, i.e., as succinate CoA transferase with promiscuous donors, acetyl-CoA and propionyl-CoA, i.e., producing acetate and propionate [48]. We are aware that the assumed substrate promiscuity of ASCT in the predicted MRO can only be verified experimentally, which is currently impossible not only for *Legendrea* but also for many other ciliate lineages.

We conclude that anaerobic spathidiids have lost their mitochondrial genome, similarly to the class Plagiopylea. Their MRO metabolism does not require a hydrogenase, making them unique among known anaerobic ciliates. The discovery of a novel anaerobic MRO in ciliates decouples canonical hydrogenase-based metabolism from core anaerobic energy conservation in the MRO. The main or exclusive prey of *L. loyezae* are multicellular gastrotrichs, and the ciliate harbors at least four stable prokaryotic symbionts. Altogether, the high completeness and careful manual annotation of essential metabolic genes provide strong support for the hypothesis of the symbiotic

consortium presented here. This is further corroborated by complementary metabolic capabilities based on transcriptomics and metagenomics, spatial distribution analysis, and ultrastructural details of the community. Our results demonstrate that single-cell imaging and omics methods are highly relevant for making in-depth metabolic predictions even for complex symbiotic systems in rare host organisms. We analyzed the most complex symbiotic consortium in a protist to date, highlighting our limited understanding of symbiotic interactions in single-cell eukaryotes. For example, we described the first *Legionellales* bacterium adapted to an anaerobic lifestyle and the most reduced member of S*yntrophaceae* (also the first such reduced symbiont in an anaerobic protist). Overall, our results reshape our understanding of anaerobic mitochondria, protist symbioses, and their co-evolution.

Materials and Methods

Cell collection

Cells of *Legendrea loyezae* and SIVAB were hand-picked with glass-drawn micropipettes from raw environmental samples (Table S5). Each cell was washed with distilled water and then either dispensed with the minimum amount of water, approximately 1 µl, into PCR tubes, which were stored at -20°C or -80°C for future processing, or fixed with 2.5% glutaraldehyde or 4% formaldehyde and consecutively processed for TEM, FIB-SEM, or FISH.

Transmission electron microscopy

Three cells of *Legendrea loyezae* were hand-picked with glass-drawn micropipettes, washed with MiliQ or distilled water, and fixed in 2.5% aqueous glutaraldehyde overnight. The cells were washed and post-fixed in 1% osmium tetroxide overnight, stained in 2.5% uranyl acetate for 2 hours, and washed. All the washes were done with distilled water. Posteriorly, the cells were dehydrated in an ethanol series: 50%, 70%, 80%, 90%, 96%, and 100% (×3) ethanol, followed by ethanol:acetone (1:1) and acetone (100% ×3). Each cell was embedded in low-viscosity resin (SPI-PON Araldite kit #02635), first in a solution 2:1 of acetone:resin for two hours, then in fresh 100% resin (×2) and left to degas in a vacuum chamber overnight. Embedded cells were polymerized at 60 °C for three days. Two of the polymerized cells were sectioned in an ultramicrotome (50-70 nm thickness) with an ultra 45° diamond knife (DiATOME, Nidau, Switzerland). Ultrathin sections were mounted on formvar-coated slot grids and observed in a transmission electron microscopes JEOL JEM-1230R and JEOL JEM-1011 (JEOL, Tokyo, Japan).

Focused Ion Beam Scanning Electron Microscopy (FIB-SEM)

The third block, containing the third embedded cell, was mounted on a stub using two-part conductive silver paint (Electron Microscopy Sciences, Pennsylvania, USA) and sputter-coated with platinum. The samples were imaged in a Helios NanoLab 650 FIB system (FEI, Eindhoven, The Netherlands), where 50-nm slices were milled with Ga ions at an acceleration voltage of 30 kV and a current of 9.4 nA. The remaining block face was then imaged with an electron current of 1.6 nA at 1.5 keV acceleration voltage at a dwell time of 6 µs using the through-the-lens backscatter-electron detector (TLD-BSE). The frame size was 6144 x 4096 pixels with a 122.88 µm horizontal field of view.

FIB-SEM data segmentation

Symbionts and MROs were segmented using ilastik v1.4.0[53] using the two-step auto-context pipeline. Predicted segmentation was exported as probabilities and exported to Microscopy Image Browser v2.9010[54], where the segmentation was checked and cleaned of artifacts. Other organelles were segmented in MIB using manual segmentation with interpolation and thresholding tools. Volumes of the models were calculated using 4/6 connectivity in MIB, then exported as .tif masks and converted to .ply models (Decimation factor 0.5) and rendered in Blender v3.5. Finally, models of each symbiont were split into single objects, and distances were calculated using 500 vertices from the surface of each symbiont to the closest point of the cell surface or other symbiont surface.

Spatial statistical analysis

Nearest-neighbor (NN) interactions between symbionts were analyzed from FIB-SEM reconstructions using two complementary null models. For each focal–target pair, we calculated the median log-transformed NN distance and the "winner fraction," defined as the proportion of focal cells for which that target was the closest of the three alternatives.

To test significance, we first applied a row-wise random-label permutation test, in which target labels were shuffled 10,000 times within each focal cell, thereby preserving the observed geometry, abundances, and crowding[55]. This produced null distributions of both statistics under the assumption of no species-specific pairing.

As a second benchmark, we implemented a complete spatial randomness (CSR) null by uniformly placing the observed numbers of each symbiont inside a three-dimensional ellipsoid with the same volume as the host cytoplasm (3.98×10^8 pix³). For 1,000 Monte Carlo replicates, the two statistics were recalculated to obtain expected means, central intervals, and p-values[56].

All analyses were performed in R v4.4.1 (R Core Team, 2025) with a custom script (https://shorturl.at/Sg1MN).

Fluorescence *in situ* hybridization

Two cells of *Legendrea loyezae* strain MOKOT were fixed in 4% paraformaldehyde for 30 min at room temperature, washed with 1× phosphate-buffered saline (PBS) for 3 min, and mounted on glass slides. Two-step permeabilization of cells was performed prior hybridization: 1) using lysozyme from chicken egg whites (Sigma-Aldrich) solution (50 mM EDTA, pH 8.0; 100 mM Tris-HCl, pH 8.0; 10 mg/ml lysozyme) for 1 hour at 37 °C, then washed in 1x PBS for 3 min, 2) using 0.5% Triton X-100 for 30 minutes at room temperature, then washed in 1x PBS for 3 min. Hybridization was performed using cyanine 3-labeled oligonucleotide probe ARC915 (5'-GTGCTCCCCCGCCAATTCCT-3') specific to all Archaea[57]. Hybridization was carried out at 46 °C for 2 hours and 40 minutes with the formamide concentration of 40%. Slides were then washed in a washing buffer (20 mM Tris-HCl, pH 8.0; 5 mM EDTA, pH 8.0; 70 mM NaCl; 0.01% SDS) at 48 °C for 15 minutes, then quickly washed in cold deionized water, and finally dipped in cold 96% ethanol. Air-dried preparations were mounted using Vectashield with DAPI (Vector Laboratories). Preparations were observed using a confocal microscope Leica TCS SP8 (equipment of the Laboratory of Confocal and Fluorescence Microscopy, Faculty of Science,

Charles University). Multiple focal Z-plane images were stacked using the Z-stack tool in the Fiji distribution of ImageJ software.

Double Labeling of Oligonucleotide Probes for Fluorescence *in-situ* Hybridization (DOPE_FISH)[58] was conducted on one cell of *Legendrea loyezae* strain 7TL using the double labeled oligonucleotides ARC915 (Atto594), DELTA495a (5'-AGTTAGCCGGTGCTTCCT-3'; Atto488)[59] with the unlabeled competitor compDelta495a (5'-AGTTAGCCGGTGCTTCTT-3')[60] and GAM42a (5'- GCCTTCCCACATCGTTT-3'; ATTO 550)[61] with the unlabeled competitor Bet42a (5'- GCCTTCCCACTTCGTTT -3'). The cell was fixed in 2% paraformaldehyde (Electron Microscopy Sciences) for 10 minutes at RT on a 3 µm IsoporeTM polycarbonate filter (Merck Millipore). The filter piece was embedded in 0.2% metaphor agarose (Lonza) and hybridized in hybridization buffer containing 35% formamide and 5 ng µL^{-1} of each probe and competitor, respectively, for 4h at 46°C. The filter was then washed for 30 minutes in 35% washing buffer at 48 °C, followed by 10 minutes wash in phosphate-buffered saline at room temperature. The filter was counterstained with 1 µg mL^{-1} 4′,6-diamidino-2-phenylindole (DAPI) for 10 minutes at 4 °C. Image stacks were recorded using a confocal laser scanning microscope (Zeiss LSM 780, 63× oil objective, 1.4 numerical aperture) and maximum intensity projected in the Zeiss Zen software.

Whole genome and transcriptome amplification

The metagenome of two cells of *L. loyezae* was amplified using REPLI-g Advanced DNA Single Cell Kit (QIAGEN) according to the manufacturer's protocol, and debranched with T7 Endonuclease (New England Biolabs, Massachusetts, USA). PCR-free libraries were prepared using the NEB Next Ultra II DNA Library kit for Illumina, and whole-genome shotgun sequencing (NovaSeqX) was performed at the OIST Sequencing section facility.

The transcriptomes of three *L. loyezae* cells and three SIVAB ciliate cells were amplified using the adapted Smart-Seq2 protocol[62]. Library preparation and shotgun sequencing (Nextera XT, NovaSeqX) were performed by Macrogen.

Genome assembly, annotation, and metabolic pathways prediction

The quality of the raw reads from whole-genome sequencing was checked using FastQC v0.11.9[63]. Bandage and BlobTools were used to previsualize and detect possible genomes[64,65]. Pair-end reads were assembled using SPAdes v4.0.0 with multiple k-mers (-k 21,33,55,77,99,127)[66].

From the assembled metagenomic contigs, we identified sequences belonging to prokaryotes using the binning pipeline BASALT v1[67]. Refinement sensitivity level was set to "deep". From the final genomic bins, we extracted full-length 16S rRNA gene sequences using Barrnap v0.9 (github.com/tseemann/barrnap) for identification and subsequent analysis[68]. Additionally, potential eukaryotic contigs were obtained from the assembly using Tiara v1.0.2[69], corroborated with Eggnog mapper[70] and NCBI Blastx annotations, and manually refined to remove all possible bacterial and prey contaminants.

The resulting MAGs of *Ca*. Methanothrix pelomyxae, *Ca.* Syntrophilus obsequens, and *Ca.* Xociella bifrons were annotated using PROKKA v1.14.6 in Galaxy server v3[71], using InterProScan v5.59-91.0[72], and EggNOG mapper[70]. Metabolic pathways were first visualized in KEGG[73] and then manually refined. The genome fragment of *Methanobacterium* sp. was

extracted manually using a custom Blast search against proteins of *M. movilense* (KF186473.1) predicted in Prokka.

Transcriptomics

Illumina adaptors were removed using fastp v0.21.0[74]. The quality of reads was checked with FastQC v0.11.9[63]. The reads were pooled together, and one reference transcriptome was assembled *de novo* using SPAdes v4.0.0[66], and proteins were translated with TransDecoder v5.5.0. The completeness was assessed with BUSCO v5.8.0 against the alveolata_odb10 dataset with the metaeuk gene predictor[75].

MRO metabolic pathway prediction and protein phylogenetic analyses

Transcripts of *L. loyzeae* were annotated using trinotate[76], and protein localization was predicted with TargetP v2.0[77] and DeepLoc v2.1[78]. The subset of transcripts predicted to be MRO-related was translated using Geneious software and searched against metagenomic (*L. loyezae*) and transcriptomic (SIVAB) datasets using BlastN. Sequence hits were manually inspected to collect homologous sequences. In parallel, published MRO proteomes of anaerobic and anaerobic ciliates[6,7,23] were searched against metagenomic and transcriptomic datasets and compared with predicted proteins, or added to the dataset, respectively. The final dataset of MRO proteins was corroborated using NCBI BLAST and IQtree phylogenetic analysis to confirm homology and ciliate origin of the proteins. When a published dataset was not available, starting datasets were constructed by BlastP searches of a seed sequence against the NR protein database (max target seqs = 100) and UniProt (Ciliophora taxon restriction). Each protein dataset was aligned using MAFFT L-INS-i (default settings), trimmed using trimal (gappyout), and trees were constructed using IQ-tree v3.0.1 under the model LG+G4 with 100 ultrafast bootstraps for branch support.

Phylogenetic analyses

16S rRNA gene sequences of the four prokaryotic symbionts of *Legendrea loyezae* were extracted from their respective genomes or transcriptomes, and nucleotide datasets were built by retrieving close relative sequences from NCBI.

18S rRNA gene sequences from *L. loyezae* and the undescribed spathidiid ciliate SIVAB were extracted from the respective metagenomes and metatranscriptomes. A dataset was built containing representatives of the class Litostomatea[26] and the NCBI nucleotide database.

The 16S and 18S rRNA gene datasets were aligned using the MAFFT G-INS-1 algorithm[79] and trimmed manually at the ends. Phylogenetic trees were constructed by the maximum likelihood (ML) method under the GTR + I + Γ as the best-fit model by ModelTest-NG according to the Akaike Information Criterion[80], and with 1,000 bootstrap pseudoreplicates for node support assessment. The ML analyses were performed in RAxML HPC v8.2.4.

References

1. Graf, J. S. et al. Anaerobic endosymbiont generates energy for ciliate host by denitrification. *Nature* **591**, 445–450 (2021).

2. Husnik, F. et al. Bacterial and archaeal symbioses with protists. *Curr. Biol.* **31**, R862–R877 (2021).
3. Stairs, C. W. et al. Anaeramoebae are a divergent lineage of eukaryotes that shed light on the transition from anaerobic mitochondria to hydrogenosomes. *Curr. Biol.* **31**, 5605-5612.e5 (2021).
4. Finlay, B. J. & Fenchel, T. An anaerobic ciliate as a natural chemostat for the growth of endosymbiotic methanogens. *Eur. J. Protistol.* **28**, 127–137 (1992).
5. Van Hoek, A. H. A. M. et al. Multiple Acquisition of Methanogenic Archaeal Symbionts by Anaerobic Ciliates. *Mol. Biol. Evol.* **17**, 251–258 (2000).
6. Lewis, W. H. et al. Convergent Evolution of Hydrogenosomes from Mitochondria by Gene Transfer and Loss. *Mol. Biol. Evol.* **37**, 524–539 (2020).
7. Rotterová, J. et al. Genomics of New Ciliate Lineages Provides Insight into the Evolution of Obligate Anaerobiosis. *Curr. Biol.* **30**, 2037-2050.e6 (2020).
8. Rotterová, J., Edgcomb, V. P., Čepička, I. & Beinart, R. Anaerobic ciliates as a model group for studying symbioses in oxygen-depleted environments. *J. Eukaryot. Microbiol.* **69**, e12912 (2022).
9. Muñoz-Gómez, S. A. Energetics and evolution of anaerobic microbial eukaryotes. *Nat. Microbiol.* **8**, 197–203 (2023).
10. Muñoz-Gómez, S. A., Kreutz, M. & Hess, S. A microbial eukaryote with a unique combination of purple bacteria and green algae as endosymbionts. *Sci. Adv.* **7**, eabg4102 (2021).
11. Méndez-Sánchez, D. et al. Methanogenic symbionts of anaerobic ciliates are host and habitat specific. *ISME J.* **18**, wrae164 (2024).
12. Fenchel, T. & Finlay, B. J. The biology of free-living anaerobic ciliates. *Eur. J. Protistol.* **26**, 201–215 (1991).

13. Takeshita, K. et al. Tripartite Symbiosis of an Anaerobic Scuticociliate with Two Hydrogenosome-Associated Endosymbionts, a *Holospora* -Related Alphaproteobacterium and a Methanogenic Archaeon. *Appl. Environ. Microbiol.* **85**, e00854-19 (2019).
14. Shinzato, N. et al. Phylogenetic Analysis and Fluorescence In Situ Hybridization Detection of Archaeal and Bacterial Endosymbionts in the Anaerobic Ciliate *Trimyema compressum*. *Microb. Ecol.* **54**, 627–636 (2007).
15. Ohkuma, M. Symbioses of flagellates and prokaryotes in the gut of lower termites. *Trends Microbiol.* **16**, 345–352 (2008).
16. Beinart, R. A., Beaudoin, D. J., Bernhard, J. M. & Edgcomb, V. P. Insights into the metabolic functioning of a multipartner ciliate symbiosis from oxygen-depleted sediments. *Mol. Ecol.* **27**, 1794–1807 (2018).
17. Treitli, S. C. et al. Hydrogenotrophic methanogenesis is the key process in the obligately syntrophic consortium of the anaerobic ameba *Pelomyxa schiedti*. *ISME J.* **17**, 1884–1894 (2023).
18. Serra, V. et al. Morphology, ultrastructure, genomics, and phylogeny of *Euplotes vanleeuwenhoeki* sp. nov. and its ultra-reduced endosymbiont "*Candidatus* Pinguicoccus supinus" sp. nov. *Sci. Rep.* **10**, 20311 (2020).
19. Gabr, A., Stephens, T. G. & Bhattacharya, D. Loss of key endosymbiont genes may facilitate early host control of the chromatophore in *Paulinella*. *iScience* **25**, 104974 (2022).
20. Coale, T. H. et al. Nitrogen-fixing organelle in a marine alga. *Science* **384**, 217–222 (2024).
21. Fenchel, T. & Finlay, B. J. Anaerobic free-living protozoa: growth efficiencies and the structure of anaerobic communities. *FEMS Microbiol. Ecol.* **7**, 269–275 (1990).
22. Boxma, B. et al. The [FeFe] hydrogenase of *Nyctotherus ovalis* has a chimeric origin. *BMC Evol. Biol.* **7**, 230 (2007).

23. Xu, J. et al. Exploring the evolution of anaerobes within ciliate class Prostomatea by transcriptomics. *Mol. Phylogenet. Evol.* **207**, 108345 (2025).
24. Roger, A. J., Muñoz-Gómez, S. A. & Kamikawa, R. The Origin and Diversification of Mitochondria. *Curr. Biol.* **27**, R1177–R1192 (2017).
25. Bu, X. et al. The energy metabolism of *Balantidium polyvacuolum* inhabiting the hindgut of *Xenocypris davidi*. *BMC Genomics* **24**, 624 (2023).
26. Pomahač, O. et al. Rediscovery of Remarkably Rare Anaerobic Tentaculiferous Ciliate Genera *Legendrea* and *Dactylochlamys* (Ciliophora: Litostomatea). *Biology* **12**, 707 (2023).
27. McCutcheon, J. P. & Moran, N. A. Extreme genome reduction in symbiotic bacteria. *Nat. Rev. Microbiol.* **10**, 13–26 (2012).
28. Liu, Y., Balkwill, D. L., Aldrich, H. C., Drake, G. R. & Boone, D. R. Characterization of the anaerobic propionate-degrading syntrophs *Smithella propionica* gen. nov., sp. nov. and *Syntrophobacter wolinii*. *Int. J. Syst. Evol. Microbiol.* **49**, 545–556 (1999).
29. Gutiérrez, G., Chistyakova, L. V., Villalobo, E., Kostygov, A. Y. & Frolov, A. O. Identification of *Pelomyxa palustris* Endosymbionts. *Protist* **168**, 408–424 (2017).
30. Chang, H., Du, B., He, K., Yin, Q. & Wu, G. Mechanistic understanding of acclimation and energy metabolism of acetoclastic methanogens under different substrate to microorganism ratios. *Environ. Res.* **252**, 118911 (2024).
31. Shu, W., Du, B. & Wu, G. Deciphering microbial responses to H2S inhibition of typical functional microorganisms in anaerobic digestion ecosystems. *Chem. Eng. J.* **513**, 162766 (2025).
32. Saini, N. & Gupta, R. S. A robust phylogenetic framework for members of the order Legionellales and its main genera (Legionella, *Aquicella*, *Coxiella* and *Rickettsiella*) based on phylogenomic analyses and identification of molecular markers demarcating different clades. *Antonie Van Leeuwenhoek* **114**, 957–982 (2021).

33. Ma, K., Weiss, R. & Adams, M. W. W. Characterization of Hydrogenase II from the Hyperthermophilic Archaeon *Pyrococcus furiosus* and Assessment of Its Role in Sulfur Reduction. *J. Bacteriol.* **182**, 1864–1871 (2000).
34. Lambrecht, J. et al. Flow cytometric quantification, sorting and sequencing of methanogenic archaea based on F420 autofluorescence. *Microb. Cell Factories* **16**, 180 (2017).
35. De Graaf, R. M. et al. The Organellar Genome and Metabolic Potential of the Hydrogen-Producing Mitochondrion of *Nyctotherus ovalis*. *Mol. Biol. Evol.* **28**, 2379–2391 (2011).
36. Smith, D. G. S. et al. Exploring the Mitochondrial Proteome of the Ciliate Protozoon *Tetrahymena thermophila*: Direct Analysis by Tandem Mass Spectrometry. *J. Mol. Biol.* **374**, 837–863 (2007).
37. Machová, I. et al. Mycobacterium tuberculosis Phosphoenolpyruvate Carboxykinase Is Regulated by Redox Mechanisms and Interaction with Thioredoxin. *J. Biol. Chem.* **289**, 13066–13078 (2014).
38. Müller, M. et al. Biochemistry and Evolution of Anaerobic Energy Metabolism in Eukaryotes. *Microbiol. Mol. Biol. Rev.* **76**, 444–495 (2012).
39. Coustou, V. et al. A Mitochondrial NADH-dependent Fumarate Reductase Involved in the Production of Succinate Excreted by Procyclic *Trypanosoma brucei*. *J. Biol. Chem.* **280**, 16559–16570 (2005).
40. Bakker, B. M. et al. Compartmentation protects trypanosomes from the dangerous design of glycolysis. *Proc. Natl. Acad. Sci.* **97**, 2087–2092 (2000).
41. Jain, P., Jain, V., Singh, A., Chauhan, A. & Sinha, S. Evaluation on the responses of succinate dehydrogenase, isocitrate dehydrogenase, malate dehydrogenase and glucose-6-phosphate dehydrogenase to acid shock generated acid tolerance in *Escherichia coli*. *Adv. Biomed. Res.* **2**, 75 (2013).

42. Harmsen, H. J., Akkermans, A. D., Stams, A. J. & De Vos, W. M. Population dynamics of propionate-oxidizing bacteria under methanogenic and sulfidogenic conditions in anaerobic granular sludge. *Appl. Environ. Microbiol.* **62**, 2163–2168 (1996).
43. Westerholm, M., Calusinska, M. & Dolfing, J. Syntrophic propionate-oxidizing bacteria in methanogenic systems. *FEMS Microbiol. Rev.* **46**, fuab057 (2022).
44. Ozuolmez, D. et al. Methanogenic archaea and sulfate reducing bacteria co-cultured on acetate: teamwork or coexistence? *Front. Microbiol.* **6**, (2015).
45. Jetten, M. S. M., Stams, A. J. M. & Zehnder, A. J. B. Methanogenesis from acetate: a comparison of the acetate metabolism in *Methanothrix soehngenii* and *Methanosarcina* spp. *FEMS Microbiol. Lett.* **88**, 181–198 (1992).
46. Chen, S. et al. Unexpected competitiveness of *Methanosaeta* populations at elevated acetate concentrations in methanogenic treatment of animal wastewater. *Appl. Microbiol. Biotechnol.* **101**, 1729–1738 (2017).
47. Lindenkamp, N., Schürmann, M. & Steinbüchel, A. A propionate CoA-transferase of *Ralstonia eutropha* H16 with broad substrate specificity catalyzing the CoA thioester formation of various carboxylic acids. *Appl. Microbiol. Biotechnol.* **97**, 7699–7709 (2013).
48. Mochizuki, K. et al. The ASCT/SCS cycle fuels mitochondrial ATP and acetate production in *Trypanosoma brucei*. *Biochim. Biophys. Acta BBA - Bioenerg.* **1861**, 148283 (2020).
49. Hackmann, T. J. Redefining the coenzyme A transferase superfamily with a large set of manually annotated proteins. *Protein Sci.* **31**, 864–881 (2022).
50. Van Grinsven, K. W. A., Van Hellemond, J. J. & Tielens, A. G. M. Acetate:succinate CoA-transferase in the anaerobic mitochondria of *Fasciola hepatica*. *Mol. Biochem. Parasitol.* **164**, 74–79 (2009).

51. De Bok, F. A. M., Stams, A. J. M., Dijkema, C. & Boone, D. R. Pathway of Propionate Oxidation by a Syntrophic Culture of *Smithella propionica* and *Methanospirillum hungatei*. *Appl. Environ. Microbiol.* **67**, 1800–1804 (2001).
52. Leger, M. M. et al. Organelles that illuminate the origins of *Trichomonas* hydrogenosomes and *Giardia* mitosomes. *Nat. Ecol. Evol.* **1**, 0092 (2017).
53. Berg, S. et al. ilastik: interactive machine learning for (bio)image analysis. *Nat. Methods* **16**, 1226–1232 (2019).
54. Belevich, I., Joensuu, M., Kumar, D., Vihinen, H. & Jokitalo, E. Microscopy Image Browser: A Platform for Segmentation and Analysis of Multidimensional Datasets. *PLOS Biol.* **14**, e1002340 (2016).
55. Diggle, P. J. *Statistical Analysis of Spatial and Spatio-Temporal Point Patterns*. (Chapman and Hall/CRC, 2013). doi:10.1201/b15326.
56. Wiegand, T. & Moloney, K. A. *Handbook of Spatial Point-Pattern Analysis in Ecology*. (Chapman and Hall/CRC, 2013). doi:10.1201/b16195.
57. Raskin, L., Stromley, J. M., Rittmann, B. E. & Stahl, D. A. Group-specific 16S rRNA hybridization probes to describe natural communities of methanogens. *Appl. Environ. Microbiol.* **60**, 1232–1240 (1994).
58. Stoecker, K., Dorninger, C., Daims, H. & Wagner, M. Double Labeling of Oligonucleotide Probes for Fluorescence *In Situ* Hybridization (DOPE-FISH) Improves Signal Intensity and Increases rRNA Accessibility. *Appl. Environ. Microbiol.* **76**, 922–926 (2010).
59. Loy, A. et al. Oligonucleotide Microarray for 16S rRNA Gene-Based Detection of All Recognized Lineages of Sulfate-Reducing Prokaryotes in the Environment. *Appl. Environ. Microbiol.* **68**, 5064–5081 (2002).
60. Lücker, S. et al. Improved 16S rRNA-targeted probe set for analysis of sulfate-reducing bacteria by fluorescence in situ hybridization. *J. Microbiol. Methods* **69**, 523–528 (2007).

61. Manz, W., Amann, R., Ludwig, W., Wagner, M. & Schleifer, K.-H. Phylogenetic Oligodeoxynucleotide Probes for the Major Subclasses of Proteobacteria: Problems and Solutions. *Syst. Appl. Microbiol.* **15**, 593–600 (1992).
62. Picelli, S. et al. Full-length RNA-seq from single cells using Smart-seq2. *Nat. Protoc.* **9**, 171–181 (2014).
63. Andrews, S. FastQC: A Quality Control Tool for High Throughput Sequence Data [Online]. (2010).
64. Laetsch, D. R. & Blaxter, M. L. BlobTools: Interrogation of genome assemblies. *F1000Research* **6**, 1287 (2017).
65. Wick, R. R., Schultz, M. B., Zobel, J. & Holt, K. E. Bandage: interactive visualization of *de novo* genome assemblies. *Bioinformatics* **31**, 3350–3352 (2015).
66. Prjibelski, A., Antipov, D., Meleshko, D., Lapidus, A. & Korobeynikov, A. Using SPAdes De Novo Assembler. *Curr. Protoc. Bioinforma.* **70**, e102 (2020).
67. Qiu, Z. et al. BASALT refines binning from metagenomic data and increases resolution of genome-resolved metagenomic analysis. *Nat. Commun.* **15**, 2179 (2024).
68. Seemann, T. barrnap 0.8 : rapid ribosomal RNA prediction. (2013).
69. Karlicki, M., Antonowicz, S. & Karnkowska, A. Tiara: deep learning-based classification system for eukaryotic sequences. *Bioinformatics* **38**, 344–350 (2022).
70. Cantalapiedra, C. P., Hernández-Plaza, A., Letunic, I., Bork, P. & Huerta-Cepas, J. eggNOG-mapper v2: Functional Annotation, Orthology Assignments, and Domain Prediction at the Metagenomic Scale. *Mol. Biol. Evol.* **38**, 5825–5829 (2021).
71. Seemann, T. Prokka: rapid prokaryotic genome annotation. *Bioinformatics* **30**, 2068–2069 (2014).
72. Jones, P. et al. InterProScan 5: genome-scale protein function classification. *Bioinformatics* **30**, 1236–1240 (2014).

73. Kanehisa, M. KEGG: Kyoto Encyclopedia of Genes and Genomes. *Nucleic Acids Res.* **28**, 27–30 (2000).
74. Chen, S. Ultrafast one-pass FASTQ data preprocessing, quality control, and deduplication using fastp. *iMeta* **2**, e107 (2023).
75. Manni, M., Berkeley, M. R., Seppey, M., Simão, F. A. & Zdobnov, E. M. BUSCO Update: Novel and Streamlined Workflows along with Broader and Deeper Phylogenetic Coverage for Scoring of Eukaryotic, Prokaryotic, and Viral Genomes. *Mol. Biol. Evol.* **38**, 4647–4654 (2021).
76. Bryant, D. M. et al. A Tissue-Mapped Axolotl De Novo Transcriptome Enables Identification of Limb Regeneration Factors. *Cell Rep.* **18**, 762–776 (2017).
77. Almagro Armenteros, J. J. et al. Detecting sequence signals in targeting peptides using deep learning. *Life Sci. Alliance* **2**, e201900429 (2019).
78. Ødum, M. T. et al. DeepLoc 2.1: multi-label membrane protein type prediction using protein language models. *Nucleic Acids Res.* **52**, W215–W220 (2024).
79. Katoh, K. MAFFT: a novel method for rapid multiple sequence alignment based on fast Fourier transform. *Nucleic Acids Res.* **30**, 3059–3066 (2002).
80. Darriba, D. et al. ModelTest-NG: A New and Scalable Tool for the Selection of DNA and Protein Evolutionary Models. *Mol. Biol. Evol.* **37**, 291–294 (2020).

Acknowledgments: We are thankful to the Viničná Microscopy Core Facility (LM2023050 Czech-BioImaging), Charles University, and the sequencing (SQC), imaging (IMG), and scientific computing (SCDA) sections from the OIST core facilities for the usage of their facilities. Computational resources were provided by the e-INFRA CZ project (ID:90254), supported by the Ministry of Education, Youth and Sports of the Czech Republic.

Funding: This work was funded by the Grant Agency of the Czech Republic, project 25-16558S (to IC), Grant Agency of Charles University, project 158624 (to OP), and the HFSP Early Career Grant RGEC29/2024; https://doi.org/10.52044/HFSP.RGEC292024.pc.gr.194160 (to FH).

Author contributions:

Conceptualization: OP, FH, IC
Methodology: OP, DMS, YHP, LMZ, MV, KK, BMH, FH
Investigation: OP, DMS, YHP, LMZ, MV, KK, BMH
Visualization: OP, DMS, YHP, LMZ, KK
Supervision: IC, FH
Writing—original draft: OP
Writing—review & editing: DMS, YHP, LMZ, MV, KK, BMH, FH, IC

Competing interests:

Authors declare that they have no competing interests.

Data and materials availability:

Sequencing data were deposited in NCBI GenBank under the BioProject XXXXXXXXXX. Raw sequencing reads were deposited on the NCBI SRA archive under the accession numbers XXXXXXXXXX. The 16S and 18S rRNA gene sequences were deposited at GenBank under the accession numbers XXXXXXXXXX. The MAGs and genomes were deposited at GenBank under the accession numbers XXXXXXXXXX. The custom scripts and pairwise distance matrices are available on GitHub: XXXXXXXXX. All other data needed to evaluate the conclusions in the paper are present in the paper and/or the Supplementary Materials. Additional data related to this paper may be requested from the authors.

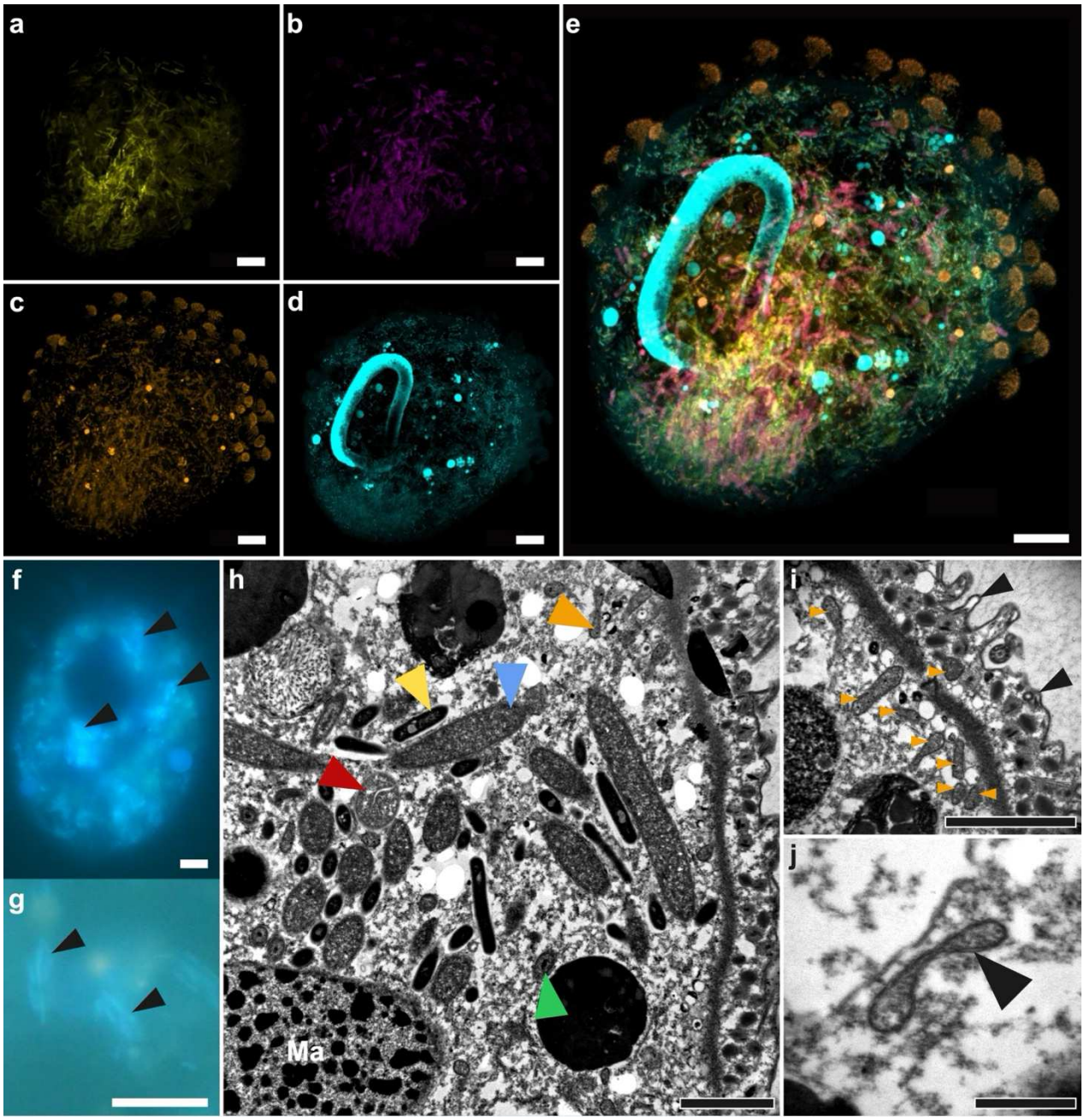

Fig. 1. Symbiotic prokaryotic consortium in *Legendrea loyezae*. a-e DOPE FISH of signals of *Ca*. Syntrophilus obsequens (Deltaproteobacteria-specific probe in a), *Ca*. Methanothrix pelomyxae (archaeal probe in b), *Ca*. Xociella bifrons (Gammaproteobacteria-specific probe in c), and the host's nucleus (DAPI staining in d), **f, g** Autofluorescence of clustered *Methanobacterium* sp. (arrowheads). **h** TEM showing spatial distribution of symbionts: *Ca*. Syntrophilus obsequens (blue), *Ca*. Methanothrix pelomyxae (red), *Ca*. Xociella bifrons (green), *Methanobacterium* sp. (yellow), and mitochondrion-related organelles (MROs; orange). **i** Localization of MROs in the periphery of the cell (orange arrowheads) close to the cell membrane (black arrowheads). **j** Ultrasctructure of the MRO without apparent cristae, but with double membrane (black arrowhead). Scale bars 10 µm (a-g), 2 µm (h, i), 0.5 µm (j).

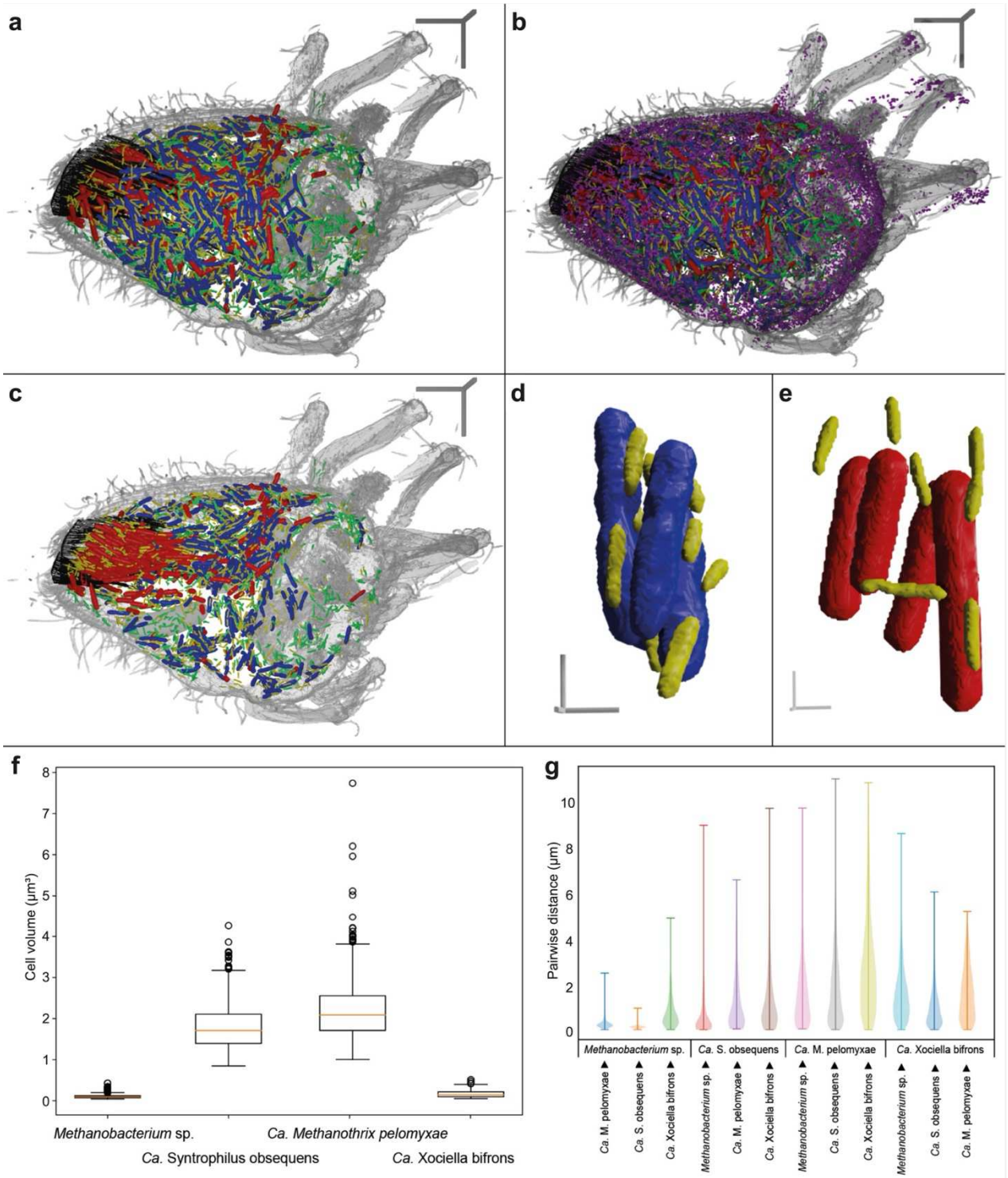

Fig. 2. 3D FIB-SEM reconstruction of *Legendrea loyezae* symbiotic consortium. a Top view of whole cell reconstruction showing four symbionts, *Ca*. Methanothrix pelomyxae (red), *Ca*. Syntrophilus obsequens (blue), *Methanobacterium* sp. (yellow), *Ca*. Xociella bifrons (green) and oral basket (black). **b** Reconstruction including the mitochondrion-related organelle (purple). **c** Transverse section of the cell showing internal arrangement. **d** Close-up view of *Ca*. S. obsequens and *Methanobacterium* sp. **e** *Ca*. M. pelomyxae and *Methanobacterium* sp. **f** Boxplot showing the volumes of each symbiont. **g** Violin plot showing the pairwise distances between symbionts. Scale bars 10 µm (a-c), 1 µm (d-e).

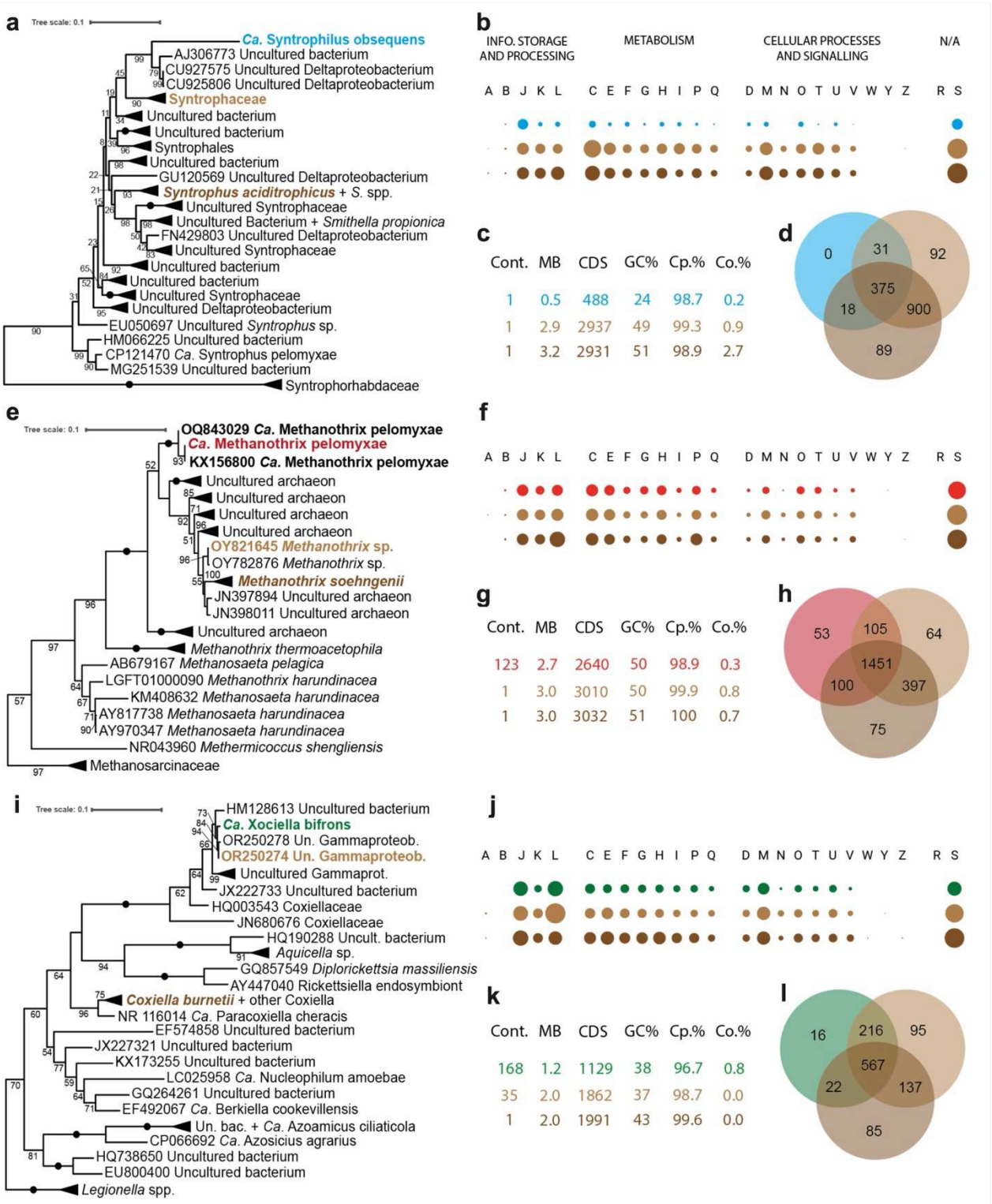

Fig. 3. Phylogenetic placement and genomic characteristics of three syntrophic prokaryotes of *Legendrea loyzae*. **a, e, i** Maximum-likelihood 16S rRNA gene trees showing the phylogenetic positions of *Ca.* Syntrophilus obsequens (blue), *Ca.* Methanothrix pelomyxae (red), and *Ca.* Xociella bifrons (green). 100 % support is shown as a filled circle. **b, f, j** Distribution of Clusters of Orthologous Groups (COG) functional categories in each metagenome-assembled genome (MAG) compared with two closely related reference genomes. Circle size corresponds to the number of genes assigned to each COG category: information storage and processing (A–L), metabolism (C–Q), and cellular processes and signaling (D–Z). **c, g, k** Summary statistics for

each MAG: number of contigs (Cont.), estimated genome size (MB), number of coding sequences (CDS), GC content (GC %), completeness (Cp. %), and contamination (Co. %). **d, h, l** Venn diagrams showing the overlap of unique and shared orthologous clusters among related genomes used for each symbiont group comparison. COG category abbreviations: Information storage and processing – [A] Translation, ribosomal structure and biogenesis; [B] Transcription; [J] Replication, recombination and repair. Cellular processes and signaling – [D] Cell cycle control, cell division, chromosome partitioning; [Y] Nuclear structure; [V] Defense mechanisms; [T] Signal transduction mechanisms; [M] Cell wall/membrane/envelope biogenesis; [N] Cell motility; [Z] Cytoskeleton; [W] Extracellular structures; [U] Intracellular trafficking, secretion and vesicular transport; [O] Post-translational modification, protein turnover, chaperones. Metabolism – [C] Energy production and conversion; [G] Carbohydrate transport and metabolism; [E] Amino acid transport and metabolism; [F] Nucleotide transport and metabolism; [H] Coenzyme transport and metabolism; [I] Lipid transport and metabolism; [P] Inorganic ion transport and metabolism; [Q] Secondary metabolite biosynthesis, transport and catabolism. Poorly characterized – [R] General function prediction only; [S] Function unknown.

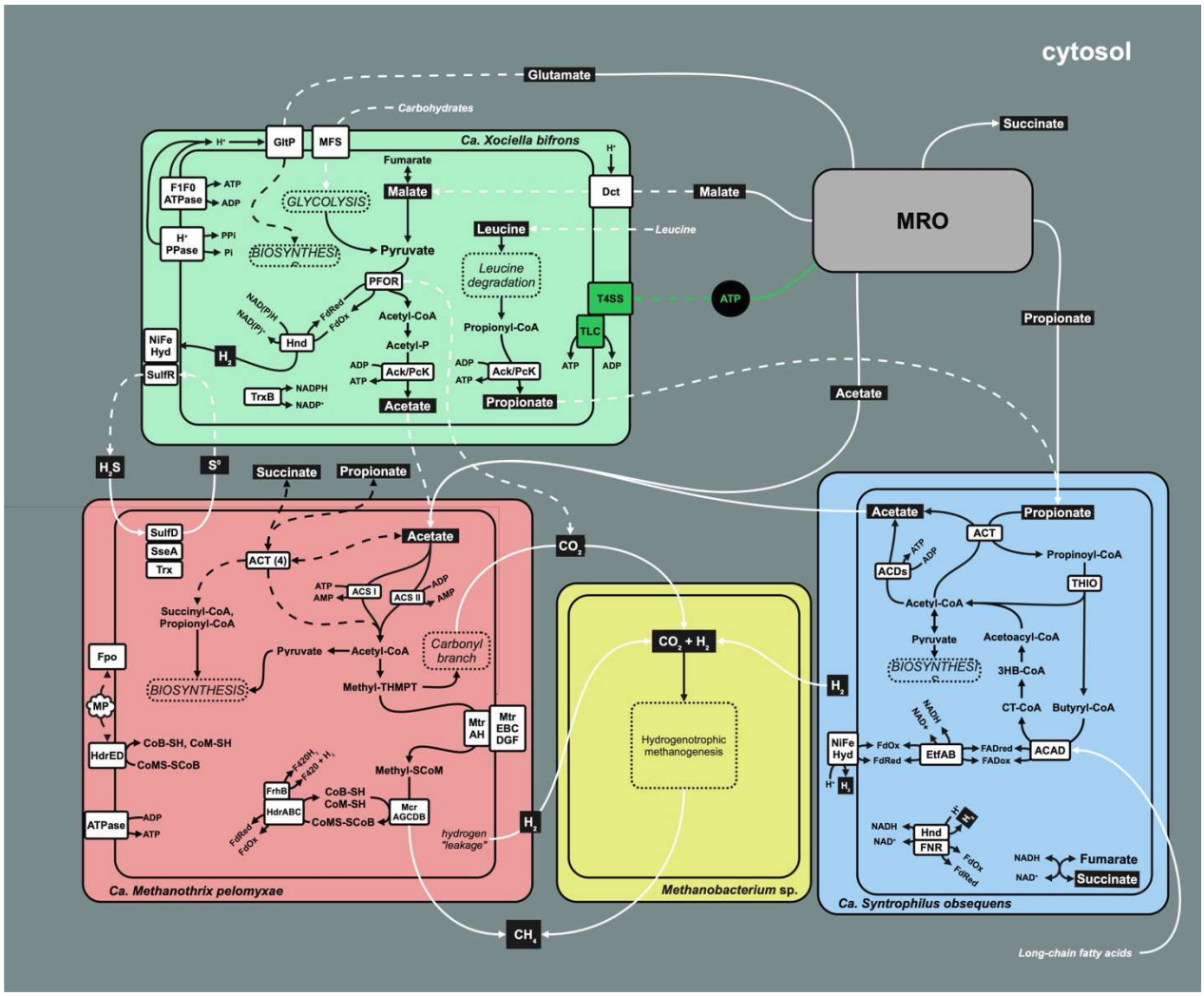

Fig. 4. Predicted metabolic network linking the novel mitochondrion-related organelle (MRO) of *Legendrea loyezae* and its four prokaryotic symbionts. Metabolic exchanges and redox interactions are inferred from genomic annotations of *Ca.* **Xociella bifrons** (green), *Ca.* **Methanothrix pelomyxae** (red), *Ca.* **Syntrophilus obsequens** (blue), ***Methanobacterium* sp,** and host **MRO.** (yellow). Dashed arrows mark uncertain or incomplete pathways; white arrows denote predicted metabolite exchange. Black arrows – internal pathways; white arrows – metabolite exchange; solid line – predictions well-supported in annotations; dashed line – uncertain predictions. Abbreviations: **PFOR** (Pyruvate:ferredoxin oxidoreductase); **Hnd** (Hydrogenase, NADH-dependent); **TrxB** (Thioredoxin reductase); **NiFe Hyd** ([NiFe]-hydrogenase); **SulfR** (Sulfide reductase); **F_1F_0 ATPase** (ATP synthase); **H^+-Ppase** (Proton pyrophosphatase); **Ack/Pck** (Acetate kinase / Phosphotransacetylase); **ACT** (Acetate-CoA transferase); **ACS** (Acetyl-CoA synthetase); **ACD** (Acyl-CoA dehydrogenase); **THIO** (Thiolase); **EtfAB** (Electron transfer flavoprotein); **FNR** (Ferredoxin–NAD^+ reductase); **Fpo** ($F_{420}H_2$ dehydrogenase); **HdrABC** (Heterodisulfide reductase complex); **FrhB** (F_{420}-reducing hydrogenase subunit B); **MtrAH** (Methyltransferase); **MtrEBCDGF** (Membrane methyltransferase complex); **MP** (Methanophenazine or related electron carrier); **SulfD** (Sulfide dehydrogenase).

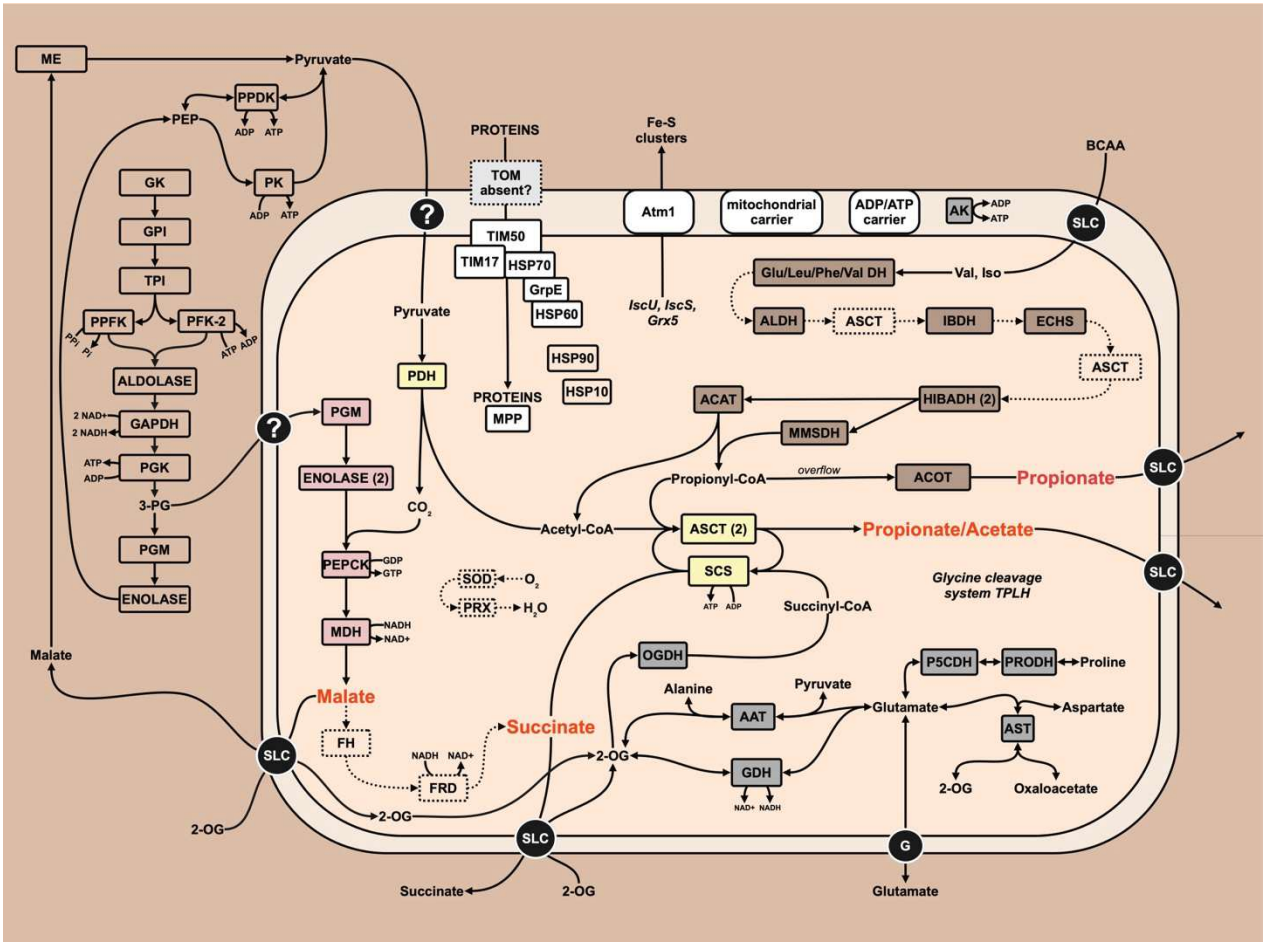

Fig. 5. Predicted metabolic pathways of the novel type of mitochondrion-related organelle of *Legendrea loyezae*. The MRO retains anaerobic carbon- and amino-acid metabolism centered on **PDH** (pyruvate dehydrogenase), **ASCT** (acetate:succinate CoA-transferase), and **SCS** (succinyl-CoA synthetase), complemented by **OGDH** (2-oxoglutarate dehydrogenase), **FH** (fumarase), **FRD** (fumarate reductase), **MDH** (malate dehydrogenase), **PEPCK** (phosphoenolpyruvate carboxykinase), **PPDK** (pyruvate phosphate dikinase), and **ME** (malic enzyme). Amino-acid degradation involves **ALDH** (aldehyde dehydrogenase), **IBDH** (isobutyrate dehydrogenase), **ECHS** (enoyl-CoA hydratase), **MMSDH** (methylmalonate semialdehyde dehydrogenase), **HIBADH** (3-hydroxyisobutyrate dehydrogenase), **ACOT** (acyl-CoA thioesterase), **ACAT** (acetyl-CoA acetyltransferase), **PRODH** (proline dehydrogenase), **P5CDH** (pyrroline-5-carboxylate dehydrogenase), **GDH** (glutamate dehydrogenase), and **AAT/AST** (alanine/aspartate aminotransferase). Cytosolic glycolytic enzymes – **GK**, **GPI**, **TPI**, **PFK**, **ALDO**, **GAPDH**, **PGK**, **PGM**, **ENO**, and **PK** – exchange metabolites with the organelle through **SLC** (solute carrier) transporters. Protein import is mediated by **TIM17**, **TIM50**, and **HSP70/HSP60/HSP90** (heat-shock proteins) in the absence of a canonical **TOM** (translocase of the outer membrane), and precursor proteins are processed by **MPP** (mitochondrial processing peptidase). The organelle retains **IscS** (cysteine desulfurase), **IscU** (scaffold protein), and **Grx5** (glutaredoxin-5) for Fe–S cluster biogenesis, with **Atm1** (ABC transporter) predicted to export Fe–S cluster intermediates to the cytosol. Minimal antioxidant defenses are represented by **SOD** (superoxide dismutase) and **PRX** (peroxiredoxin). Dashed arrows mark incomplete reactions; orange labels denote predicted metabolic outputs (malate, succinate, propionate).

Supplementary Files

This is a list of supplementary files associated with this preprint. Click to download.

- SupplementaryMaterials.pdf
- TableS1.Symbiontsspatialstatisticsanalysis.xlsx
- TableS2Contaminantsinmetagenomicandtranscriptomicdata.xlsx
- TableS3.AnnotatedputativeMethanobacteriumsp.proteinsinvolvedinmethanogenesis.xlsx
- TableS4.LegendreaLoyezeaeMROtargetingpredictiontables.xlsx
- MovieS1.3DmodelofLegendrealoyezaeandtheirprokaryoticsymbionts.avi
- FigureS5MitochondrialrelatedorganelleMROsingleproteintreescollection.pdf